

Ecological Driving System for Connected/Automated Vehicles Using a Two-Stage Control Hierarchy

Ke Huang, *Member, IEEE*, Xianfeng Yang^{ID}, Yang Lu, Chunting Chris Mi, *Fellow, IEEE*, and Prathyusha Kondlapudi

Abstract—To improve a vehicle’s fuel efficiency when operating on roadways, this study develops an ecological driving system under the connected and automated vehicle (CAV) environment. The system includes three critical functions, including traffic state prediction, eco-driving speed control, and powertrain control implementation. According to the real-time traffic information obtained from vehicle-to-infrastructure and vehicle-to-vehicle communications, the embedded traffic state prediction model will estimate and predict the average speeds and densities of freeway subsections. With an objective of minimizing the fuel consumption, the eco-driving speed control function follows a two-stage hierarchical framework. The first stage, which is executed at the global level, aims to optimize the travel speed profile of the CAV over a certain time period. The second stage, local speed adaption, is designed to dynamically adjust the CAV’s speed and make lane-changing decisions based on the local driving condition. The resulting control parameters will then be forwarded to the powertrain control system for implementations. To evaluate the proposed system, this study performs comprehensive numerical tests by using simulation models. This results confirm the effectiveness of the proposed system in reducing fuel consumption. Further comparisons with different models highlights the need to consider traffic state information in the first-stage optimization and lane-changing decision module in the local adaption function.

Index Terms—Eco-driving, connected and automated vehicle (CAV), traffic state prediction, fuel consumption minimization, two-stage control hierarchy.

I. INTRODUCTION

ACCORDING to the U.S. Department of Transportation (USDOT) surveys, transportation sector consumes 28% of total energy to move people and goods in the United States [1]. Despite the existence of many transportation modes such as personal cars, buses, trucks, trains, airplanes, and ships, so far the largest share of energy consumption is from cars and light trucks [2]. Hence, improving vehicle’s fuel

efficiency becomes a vital issue in transportation engineering. Although drivers’ behaviors are commonly recognized as one of the most important factors [3] that affects energy consumption, the design of powertrain operational systems also play a key role in improving fuel efficiency.

In response to such a need, a large amount of studies have reported their methodologies to design ecological driving system, which aims to operate vehicles in an energy efficient way. Early studies developed the so called “eco-cruise control” system which dynamically adjust cruise speed based on the roadway grade information [4]. To operate vehicles in a more complex environmental, more recent studies focused on the design of eco-oriented driving systems which can optimize vehicle speed profile in real time. The most pioneer works in such field have been conducted on single vehicles. Notably, some field experiments have highlighted the potential benefits of eco-driving systems on reducing vehicles’ fuel consumption [5]–[9]. In review of the literature, a group of researchers developed a set of speed optimization algorithms that allow vehicles to adjust their travel speeds within a specified range [10], [11]. By accounting for the topography information, those systems enable vehicles to use the energy gained from downhill roadway sections to overcome the grade resistance on uphill sections. Similarly, another group reported their algorithms in optimizing vehicle trajectories [12], [13] and several studies extended the control logic to heavy vehicles [14]. However, these aforementioned studies may fall short of effectiveness due to the lack of real-time traffic information.

Recent technology advancement on connected and automated vehicles (CAVs) provides the possibility of integrating real-time traffic information into an eco-driving system. With on-board communication devices, connected vehicles are allowed to exchange information with other vehicles (V2V), roadside infrastructure (V2I), and the “Cloud” (V2C). Fully automated vehicles are defined by National Traffic Safety Administration (NHTSA) as those in which operation of the vehicle occurs without direct driver input to control the steering, acceleration, and braking and are designed so that the driver is not expected to constantly monitor the roadway while operating in self-driving mode. Using CAV technologies, existing studies have reported various models to improve the efficiency of eco-driving systems. According to [15], those studies can be classified into two categories: vehicle speed/acceleration control and powertrain control. The first

Manuscript received May 18, 2017; revised October 23, 2017 and February 28, 2018; accepted March 1, 2018. Date of publication March 20, 2018; date of current version June 28, 2018. The Associate Editor for this paper was R. Malekian. (*Corresponding author: Xianfeng Yang.*)

K. Huang, C. C. Mi, and P. Kondlapudi are with the Department of Electrical and Computer Engineering, San Diego State University, San Diego, CA 92182 USA (e-mail: k Huang@mail.sdsu.edu; cmi@mail.sdsu.edu; kprathyusha8@gmail.com).

X. Yang is with the Department of Civil and Environmental Engineering, The University of Utah, Salt Lake City, UT 84112 USA (e-mail: x.yang@utah.edu).

Y. Lu is with Transportand ICT, World Bank, Washington, DC 20433 USA (e-mail: karlluyang@gmail.com).

Color versions of one or more of the figures in this paper are available online at <http://ieeexplore.ieee.org>.

Digital Object Identifier 10.1109/TITS.2018.2813978

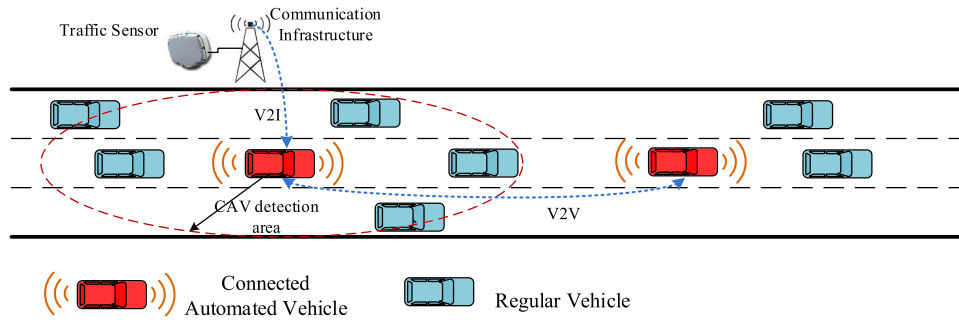


Fig. 1. The illustration of CAV operational environment

category of studies aimed at optimizing the speed profile and acceleration rate so as to minimize the fuel consumptions. Those optimization models are developed with various control objectives such as intelligent merging [16], [17], platooning [18]–[20], and eco-approaching [21], [22]. The second category focused on the real-time optimization of key parameters in vehicles powertrain system [23]–[25] where regular vehicles, electric vehicles, and hybrid vehicles are all studied by various researchers.

After obtaining the real-time information, it is always critical to explore efficient computational algorithms in the optimization process since CAVs need to be safely operated in response to the change of travel environment. A group of researchers used dynamic programming (DP) as the tool to solve the nonlinear models with complex constraints [26], [27]. While DP was proven to be effective, its computation time is still too long for real-time operations. To overcome this issue, other studies developed Model Predictive Control (MPC) with quadratic programming technique [28] and Legendre Pseudospectral method [29]. However, those approaches are only capable of dealing with a relatively short time horizon due to limitations caused by the computational efficiency requirement. The short horizon, which can satisfy the on-line operation need, generally produces less optimized solution from the long-term aspect.

To fully account for the benefit of long-term optimization and the computation efficiency of short-term operations, reference [30] developed a two-stage hierarchy in designing distance-based ecological driving system. Using the speed limit as the target speed, the first stage of their control framework, named “long-term optimization”, is used to find the most energy-efficient speed profile between the vehicle’s origin and destination. Such optimization is done before the departure of vehicles. Then based on the obtained speed profile, the second stage named “local adaptive” is used to dynamically adjust vehicle’s speed according to real-time driving condition (e.g., the speed and location of nearby vehicles). Despite the effectiveness of such two-stage control hierarchy in reducing energy consumption, the entire optimization process is operated with a single vehicle and real-time traffic condition is not taken into account.

In this study, we will explore the potential of introducing vehicle automation and connectivity into the two-stage hierarchy. The main contributions of this work are summarized

as follows: 1) developing an eco-CAV operational framework which allows the target CAV to take into account real-time traffic information for powertrain optimization; 2) integrating traffic state prediction function and implementing such information with a rolling-horizon control logic; and 3) providing a lane-changing decision function in the local adaption stage to further improve fuel efficiency.

The remaining of this paper is organized as follows. Section II will introduce the CAV operational environment and illustrate the control framework of the proposed eco-driving system. Section III will present the details of model formulation in the three key steps: traffic state prediction, long-term speed profile optimization, and local adaption. Section IV will show the system evaluation with numerical examples and Section V will conclude the paper.

II. ECOLOGICAL DRIVING SYSTEM ARCHITECTURE

A. CAV Operational Environment

The connectivity technology of CAVs allows the exchange of traffic information between vehicles and infrastructure. The vehicle automation function will automatically adjust the speed in real time through the optimization of the powertrain system. As shown in Fig. 1, roadside traffic sensors are able to collect the traffic data such as flow rate (number of vehicles) and average vehicle speed. Through the communication infrastructure, data from multiple neighboring sensors will be recorded and sent to CAVs (V2I). Then the computational devices on CAVs can perform computational works based on the real-time data. For the need of vehicle automation, it always requires reliable sensors on automated vehicles. Three major types of sensors are used in practice, including radar, LiDAR, and camera. With the integration and coordination of different types of sensors, the automated vehicles can be aware of the locations and speeds of surrounding vehicles. Such detected information can be further sent to other nearby CAVs through the V2V communication platform. By integrating the connectivity technology with vehicle automation, the proposed ecological driving system in this study can guarantee its operational effectiveness even with a low penetration rate of CAVs.

B. Proposed System Architecture

Fig. 2 shows an overview of the proposed two-stage eco-driving optimization framework. The traffic state model will

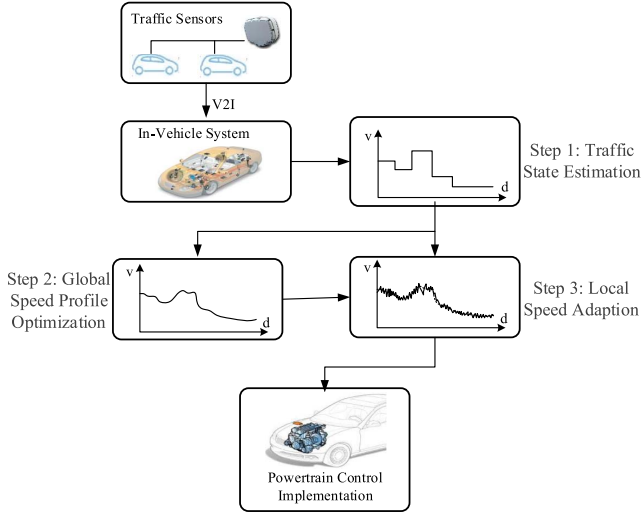


Fig. 2. Illustration of the system architecture.

yield a prediction of the freeway traffic condition using real-time traffic information. Let S denote the total travel distance between the target CAV's origin and destination, and n denote the number of distance segments. At any given time t , the traffic state model predicts the average traffic speed profile for each of the n distance steps $\hat{V}(s, t) = [\hat{V}(s_1, t), \dots, \hat{V}(s_n, t)]$, where $\hat{V}(s_i, t)$ denotes predicted average traffic flow speed at the i -th distance segment and s_i denotes the i -th distance segment. The advantage of using $\hat{V}(s, t)$ as the reference in our model is twofold: first, average traffic flow speed profile prediction allows us to consider realistic traffic condition, whereas considering only speed limit on a specific road section for optimization would result in too optimistic speed profile and cause abrupt speed reductions when local adaption is performed; second, the prediction model takes into account time-varying traffic state. As will be shown later, by using the rolling horizon control logic, we can periodically refresh the predicted speed profile $\hat{V}(s, t)$ to take into account the most up-to-date traffic state information.

The predicted real-time traffic speed profile is then communicated to the CAV through V2I channel and will be used as input information for long-term global eco-driving optimization, as illustrated in Step 2 of Fig. 2. In this step, the system optimizes powertrain control parameters such as engine torque and brake force with an objective of minimizing vehicle's fuel consumption. Several constraints, such as speed constraints derived from previously estimated global average speed profile $\hat{V}(s, t)$ and road conditions, etc. are taken into account. The optimized powertrain control parameters will be further used to compute the speed profile on each of the n distance steps: $V_{opt}(s, t) = [V_{opt}(s_1, t), \dots, V_{opt}(s_n, t)]$. Details on global long-term optimization will be discussed in Section III-B.

The second step of the two-stage hierarchical framework is dynamic local speed adaption, which uses optimized long-term speed profile $V_{opt}(s, t)$ as a reference in the optimization, as shown in Step 3 of Fig. 2. However, during the course of driving, unpredictable events may interrupt driving and

 TABLE I
 LIST OF PARAMETERS CONSIDERED IN THIS STUDY

Symbol	Definition
A, B, C, D, X	Vehicle speed state equation parameters
A_d	Frontal area of the vehicle
$\beta_1, \beta_2, \gamma_1, \gamma_2$	Fuel rate model parameters
C_1, C_2, C_3	Vehicle parameters
C_d	Drag coefficient
C_r	Rolling resistance coefficient
d_i	Distance from the preceding vehicle at i -th time point
$d_{i,adj}$	Distance from the preceding vehicle in
$d_{i,follow}$	Threshold distance for following global target optimized speed profile the adjacent lane at i -th time point
D_c	Critical density in traffic state model
$D_i(t)$	Mean traffic density for i -th segment at t
ΔD_t	Safety distance
F_{brake}	Brake force
f_r	Final drive ratio
g	Gravity
g_r	Gear ratio
h, l, V_m	Safety distance model parameters
J	Fuel consumption
m	Vehicle mass
$\dot{m}_f(t)$	Instantaneous mass fuel rate
n	Number of distance segments
n_i	Total number of subsections in the traffic state prediction model
N_{fr}	Efficiency of the final drive
N_{gr}	Efficiency of gear box/torque converter
n_r	Gear number
$q_i(t)$	Transition flow rate to segment $(i + 1)$ at t
ρ	Air density
$r_i(t)$	On-ramp flow rate to segment i at t
$r_w(t)$	Wheel radius
Δs	Distance of each segment
$s_i(t)$	Off-ramp flow rate leaving segment i at t
S	Total traveling distance
T_e	Engine torque
θ	Road grade
t	Traveling time
u	Instantaneous powertrain control parameter vector
U	Global powertrain control parameter vector
$\hat{V}(s_i, t)$	Predicted average traffic speed for i -th segment
$V_{opt}(s_i, t)$	Optimized global speed for i -th segment
w_1, w_2	Weight parameters in the optimization
ω_e	Engine rotational speed
v	Vehicle velocity
$\nu, \tau, \kappa, \alpha$	Traffic state parameters

prevent the vehicle from following long-term speed profile. For example, preceding neighboring vehicles from other lanes may suddenly change to the CAV's lane and consequently result in potential traffic accidents. In this case, it is critical to dynamically adapt the instantaneous speed profile to maintain safety distance. Thus, during local adaption, optimization is performed repeatedly by taking into account local road perturbations and safety driving distance as dynamic constraints. More details on local adaption will be discussed in Section III-B. In the following section, we will discuss details of constituent blocks in the proposed system architecture.

III. MODEL DEVELOPMENT

In this Section, we will show the details of our eco-driving model. Table I provides a summary of vehicle and model parameters considered in this manuscript.

A. Traffic State Prediction

The first step of the proposed system is the prediction of current traffic state. To provide traffic state (speed and density) as input to the two-stage eco-driving control hierarchy, it is essential to predict the traffic state evolution on the target roadway sketched over a projected time horizon. In this work, we employ a macroscopic traffic flow model to predict the flow rate, average speed, and density. As discussed before, the target roadway segment is divided into n segments with a unit length of $\Delta s = S/n$. When dividing a freeway segment, the length of each segment should be sufficiently long so that vehicles cannot pass one subsection during one time interval. Moreover, each subsection is allowed to have at most one on-ramp and one off-ramp. For the i -th segment at a given time t , the mean density $D_i(t)$ can be determined by the difference between the input and output flows as follows:

$$D_i(t+1) = D_i(t) + \frac{\Delta T}{\Delta s \times n_i} [q_{i-1}(t) - q_i(t) + r_i(t) - s_i(t)] \quad (1)$$

where $q_i(t)$ denotes transition flow rate entering segment $(i+1)$ from segment i at t , $r_i(t)$ denotes the on-ramp flow rate entering segment i at t , $s_i(t)$ denotes the off-ramp flow rate leaving segment i at t , n_i is the total number of lanes, and ΔT denotes the unit time interval to update the traffic flow model. The transition flow rate is determined by:

$$q_i(t) = D_i(t) \times \hat{V}(s_i, t) \times n_i \quad (2)$$

To dynamically update the average speed, $\hat{V}(s_i, t)$, a well-developed equation proposed by [31] in their METANET model is adopted and shown as follows:

$$\begin{aligned} \hat{V}(s_i, t+1) = & \hat{V}(s_i, t) + \frac{\Delta T}{\tau} \{V[D_i(t)] - \hat{V}(s_i, t)\} \\ & - \frac{\Delta T}{\Delta s} \hat{V}(s_i, t) [\hat{V}(s_{i-1}, t)] \\ & - \frac{v \cdot \Delta T}{\tau \cdot \Delta s} \frac{D_{i+1}(t) - D_i(t)}{D_i(t) + \kappa} \end{aligned} \quad (3)$$

where $V[D_i(t)]$ is the static speed for segment i at time t with respect to the density:

$$V[D_i(t)] = u_f \cdot \exp\left[-\frac{1}{\alpha} \left(\frac{D_i(t)}{D_c}\right)^\alpha\right] \quad (4)$$

and v , τ , κ , α are traffic state model parameters and D_c is the critical density. Using the macroscopic traffic flow model (Eqs. 2-4), the system can predict the average speed of each sub-segment i over projected time horizon. Since the model is implemented with an assumption that the detected traffic flow pattern remains unchanged overtime, the long-term prediction may not be accurate enough for applications when the distance between vehicle's origin and destination is long. Hence, instead of performing a one-time traffic prediction before the departure of vehicle, this study employs the rolling-horizon control logic in the eco-driving system. As shown in Fig. 3, a long-term prediction will be carried out before the departure of vehicle and the resulting traffic state (#1) will be implemented as the input of two-stage hierarchy model. Once the vehicle approaches a new communication infrastructure,

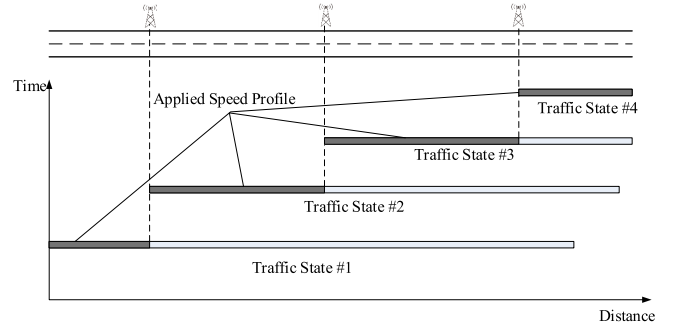


Fig. 3. The rolling-horizon control logic.

new data from traffic sensors will be available through V2I communication. At this time, another traffic state prediction based on updated data will be executed and the new traffic state (#2) will be used as input. Such procedure will be repeated until the vehicle reaches its destination. By using the rolling-horizon framework, the proposed eco-driving system can fully take advantage of the benefit of CAV technology and utilize most updated information for optimization.

B. Long-Term Optimization

The predicted traffic flow will then serve as the baseline for our two-stage hierarchical model to minimize fuel consumption under various traffic condition constraints. The goal is to dynamically estimate control of powertrain parameters in order to minimize fuel consumption based on several considerations: i) average traffic flow profile derived from our traffic state prediction model ii) speed constraints and road conditions, iii) neighboring vehicle distance and speed.

1) *Fuel Consumption Formulation*: The long-term optimization serves as global model to estimate most energy-efficient powertrain control states for a predefined traveling distance, denoted by S . The optimization takes into account average traffic flow speed profile derived from our traffic state prediction model $\hat{V}(s, t) = [\hat{V}(s_1, t), \dots, \hat{V}(s_n, t)]$. Specifically, the fuel consumption cost given a time window $[t_0, t_f]$ can be expressed as shown in [24]:

$$J = \int_{t_0}^{t_f} \dot{m}_f(t) dt \quad (5)$$

where $\dot{m}_f(t)$ denotes instantaneous mass fuel rate (kg/s) which is a function of powertrain control input vector $\vec{u}(t) = [T_e(t), \omega_e(t)]$, where T_e is the engine torque and ω_e is the engine rotational speed. In this work, we adopt Willans line approximation [32] for expressing $\dot{m}_f(t)$ and use the distance-based fuel consumption expression in [30] to further express J as:

$$\begin{aligned} J = \sum_{k=0}^{n-1} & \left((\beta_1 f_r g_r(n_r)/r_w + \beta_2) \cdot T_e(k) \right. \\ & \left. + \gamma_1 f_r g_r(n_r)/r_w + \gamma_2 \right) \Delta s \end{aligned} \quad (6)$$

where $\beta_1 = 5.646 \times 10^{-8}$, $\beta_2 = 4.751 \times 10^{-7}$, $\gamma_1 = 1.625 \times 10^{-6}$, $\gamma_2 = -5.968 \times 10^{-5}$, $v(k)$ denotes vehicle velocity (m/s) at k -th segment, r_w denotes wheel radius, f_r is

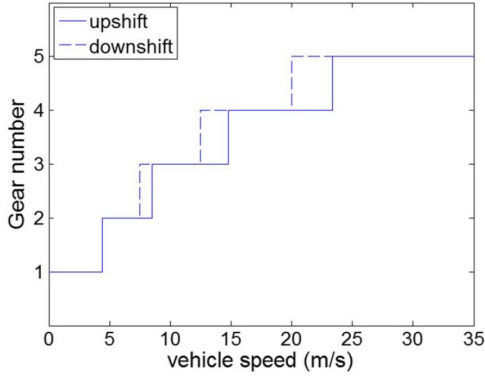


Fig. 4. Gear shift rules.

the final drive ratio and $g_r(n_r)$ is the gear ratio given a gear number n_r , which is determined by the gear shifting rules as specified in Fig. 4, and Δs is the distance of each segment: $S = \Delta s \times n$. According to [30], the state equation for the speed at k -th segment can be expressed as:

$$v(k)^2 = \left(1 - \frac{2C_2\Delta s}{m}\right)v(k-1)^2 + \left[\frac{2C_1\Delta s}{m}, -\frac{2\Delta s}{m}\right] \begin{bmatrix} T_e(k-1) \\ F_{brake}(k-1) \end{bmatrix} - \frac{2C_3\Delta s}{m} \quad (7)$$

where m denotes the mass of the vehicle (kg), F_{brake} denotes the brake force applied at one segment, C_1 , C_2 and C_3 are vehicle parameters defined as:

$$C_1 = \frac{f_r g_r(n_r) N_{f_r} N_{g_r}(n_r)}{r_w} \quad (8)$$

$$C_2 = \frac{1}{2} \rho C_d A_d \quad (9)$$

$$C_3 = m \cdot g \cdot C_r \cos \theta(k) + m \cdot g \cdot \sin \theta(k) \quad (10)$$

where N_{f_r} denotes the efficiency of the final drive, $N_{g_r}(n_r)$ denotes the efficiency of a gear box and a torque converter which is a function of the gear number, an input speed, and an input torque, and it is modeled as the product of the gearbox efficiency and the torque converter efficiency, ρ denotes the air density (kg/m^3), C_d denotes the drag coefficient, A_d denotes the frontal area of the vehicle (m^2), g is the gravity (m/s^2), C_r is the rolling resistance coefficient, and $\theta(t)$ is the road grade (rad). For a given vehicle

and a predefined traveling distance, assume that the initial velocity is $v(0)$, and let the vector U denote the powertrain control parameters applied on all segments of the entire traveling distance: $U = [T_e(0), F_{brake}(0), \dots, T_e(n-1), F_{brake}(n-1)]$, then the fuel consumption optimization search algorithm consists of computing the optimal value of U_{opt} in the $(2 \times n)$ -dimensional space that minimizes the total fuel consumption J .

2) *Fuel Consumption Optimization With Constraints:* In order to consider velocity profile as our optimization constraints, we need to express velocity as a function of our optimization parameter vector U . In this work, we use the expression shown in [30] to rewrite equation (7) as:

$$X(k+1) = A(k)X(k) + B(k)u(k) - D(k) \quad (11)$$

where $X(k) = v(k)^2$, $A(k) = 1 - \frac{2C_2\Delta s}{m}$, $B(k) = [\frac{2C_1\Delta s}{m}, -\frac{2\Delta s}{m}]$, $u(k) = [T_e(k), F_{brake}(k)]^T$, $D(k) = \frac{2C_3\Delta s}{m}$. Then the vehicle longitudinal states for all segments can be expressed in matrix form as shown in (12), as shown at the bottom of this page.

We can then use matrix notations \bar{A} , \bar{B} , U , \bar{C} and D to rewrite Equation (12):

$$X = \bar{A}X(0) + \bar{B}U + \bar{C}D \quad (13)$$

We can manipulate equation (13) as the following:

$$\bar{B}U = X - \bar{A}X(0) - \bar{C}D \quad (14)$$

Equation (14) allows us to impose linear equalities to global fuel consumption optimization based on predicted average traffic speed profile $\hat{V}(s, t)$. The global fuel consumption optimization can be then formulated as following:

$$\begin{aligned} \min_U \sum_{k=0}^{n-1} & \left((\beta_1 f_r g_r(n_r)/r_w + \beta_2) \cdot T_e(k) \right. \\ & \left. + \gamma_1 f_r g_r(n_r)/r_w + \gamma_2 \right) \Delta s \\ \text{subject to } & 0 \leq U \leq U_{max} \\ & \begin{bmatrix} -\bar{B} \\ \bar{B} \end{bmatrix} U \leq \begin{bmatrix} -(X_{min} - \bar{A}X(0) - \bar{C}D) \\ X_{max} - \bar{A}X(0) - \bar{C}D \end{bmatrix} \end{aligned} \quad (15)$$

where U_{max} denotes the upper boundary of powertrain control parameter, X_{min}/X_{max} is speed lower/upper boundary. The global optimization formulated in (15) provides optimal

$$\begin{aligned} X = \begin{bmatrix} X(0) \\ X(1) \\ \vdots \\ X(n-2) \\ X(n-1) \end{bmatrix} &= \begin{bmatrix} 1 \\ A(0) \\ \vdots \\ A(n-3) \cdots A(0) \\ A(n-2) \cdots A(0) \end{bmatrix} X(0) + \begin{bmatrix} 0 & 0 & \dots & 0 & 0 \\ B(0) & 0 & \dots & 0 & 0 \\ A(1)B(0) & B(1) & \dots & 0 & 0 \\ \vdots & \vdots & \vdots & \vdots & \vdots \\ A(n-2) \cdots A(1)B(0) & A(n-2) \cdots A(2)B(1) & \dots & B(n-2) & 0 \end{bmatrix} \\ &+ \begin{bmatrix} T_e(0) \\ F_{brake}(0) \\ \vdots \\ T_e(n-1) \\ F_{brake}(n-1) \end{bmatrix} + \begin{bmatrix} 0 & 0 & \dots & 0 & 0 \\ 1 & 0 & \dots & 0 & 0 \\ \vdots & \vdots & \vdots & \vdots & \vdots \\ A(n-3) \cdots A(1) & A(n-3) \cdots A(2) & \dots & 0 & 0 \\ A(n-2) \cdots A(1) & A(n-2) \cdots A(2) & \dots & 1 & 0 \end{bmatrix} \begin{bmatrix} D(0) \\ D(1) \\ \vdots \\ D(n-2) \\ D(n-1) \end{bmatrix} \end{aligned} \quad (12)$$

powertrain control that minimizes fuel consumption for a given driving distance S by taking into account road condition and predicted global traffic speed profile. Note that global traffic speed profile is dynamically predicted and can be updated periodically to reflect global traffic flow change. In such case, global optimization formulated in (15) is also performed periodically using rolling horizon control logic to ensure updated global optimal powertrain control. In this work, we use genetic algorithm (GA) for long-term global optimization. The details of GA is discussed in the following section.

3) *Genetic Algorithm for Global Optimization*: Due to the non-differentiable and discontinuous nature of the global optimization formulation in (15), we employ GA in this work for fast and efficient global search for long-term global optimization. GA aims at solving both constrained and unconstrained optimization problems by iteratively modifying a population of individual solutions. Lower/upper boundaries and linear constraints shown in (15) are handled at each iteration throughout the optimization. GA uses the mutation and crossover functions to produce new individuals at every generation. Only feasible new points are generated with respect to the linear and bound constraints. Once the optimal powertrain control parameters U_{opt} is obtained, we can easily reconstruct the corresponding speed profile using:

$$V_{opt} = \sqrt{\bar{A}X(0) + \bar{B}U_{opt} + \bar{C}D} \quad (16)$$

C. Local Adaption

While following the predetermined global reference speed profile V_{opt} , we should also consider local unpredictable perturbations, e.g., a sudden change of lane of vehicles on adjacent lane or a sudden slowdown of the preceding vehicle, to ensure safety driving distance. To account for local perturbations on the road, we propose a local adaptation technique that detects the distance from the preceding vehicle at real time, and adapt local speed profile if necessary to ensure safety distance.

Fig. 5 illustrates the local speed adaption flow based on real-time preceding vehicle speed, computed safety distance, and global optimal speed profile. The local speed adaption is performed on a time-based driving cycle, i.e., adaption is repeatedly performed at every time step Δt , usually very small, to ensure safety driving distance. At i -th time step, the distance from the preceding vehicle, denoted by d_i as well as that from the preceding vehicle on the adjacent lane, denoted by $d_{i,adj}$ are computed. Note that d_i and $d_{i,adj}$ can be measured and estimated by in-vehicle sensing devices such as image sensors, laser radar, and millimeterwave radar. The safety distance ΔD_t at i -th time step t_i can be then computed based on the current vehicle speed:

$$\Delta D_t = h \times v(t_i) + l \quad (17)$$

where h and l are constants whose values can be set to 2 according to [30] and $v(t_i)$ is the instantaneous speed at time t_i . Based on the computed safety distance, we set a threshold distance d_{follow} such that if $d_i \geq d_{follow}$, then we consider the vehicle is in safe mode and the speed at time step

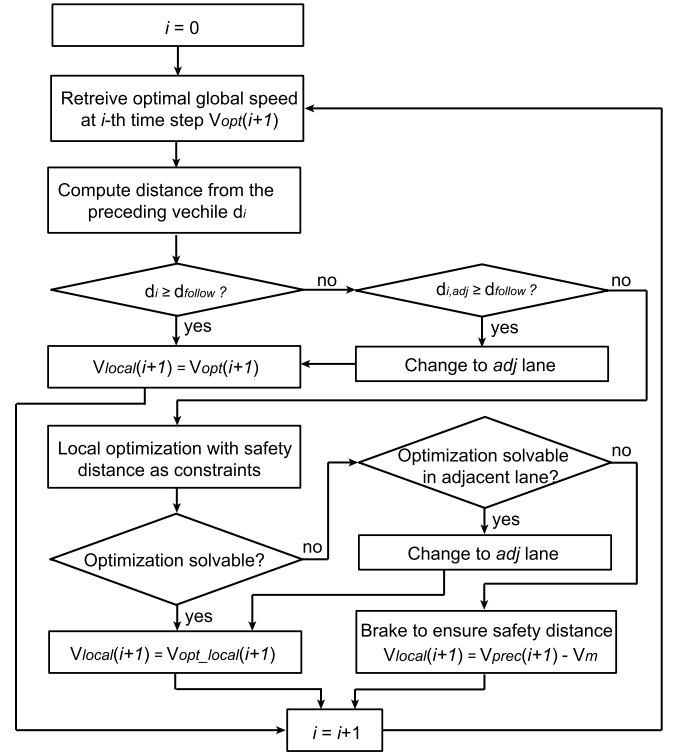


Fig. 5. Local speed adaption flow.

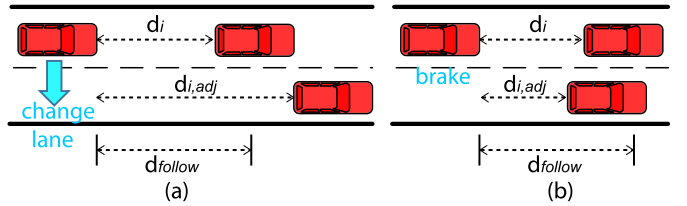


Fig. 6. Example illustration of local adaption when (a) lane change is needed, and (b) local adaption is unsolvable in both lanes and brake is needed.

t_i should follow the optimized global speed $V_{opt,i}$, which is obtained by a simple distance-to-time speed profile conversion. Meanwhile, the distance from the preceding vehicle on the adjacent lane $d_{i,adj}$ is also detected. If $d_i < d_{follow}$ and $d_{i,adj} \geq d_{follow}$, then the vehicle will change from the current lane to the adjacent lane and follow the optimized global speed $V_{opt,i}$. Note that in this work, we assume one adjacent lane, and this method can be easily extended to the case of 2 adjacent lanes. An example of lane change situation is illustrated in Fig. 6(a). If $d_i < d_{follow}$ and $d_{i,adj} < d_{follow}$, then there is a risk of safety distance violation given that the current distance is closer to ΔD_t . In this case, we perform local optimization using optimized global speed profile as target and ΔD_{t+1} as additional constraints for safety distance. As shown in [30], by neglecting constant terms and terms with small variations, the cost function in local optimization can be expressed as the following quadratic notation:

$$J_{cost,i} = w_1 \cdot K \cdot u(i) + w_2 \cdot (u(i)^T B(i)^T B(i) u(i) - 2B(i)u(i) \cdot V_{opt,i+1}^2) \quad (18)$$

where w_1 and w_2 are weight values associated with each optimization goal, and K is the vector defined as $K = [\frac{\beta_1 f_r g_r (n_r) \Delta s}{r_w} 0]$. Thus local optimization can be expressed as quadratic programming form:

$$\begin{aligned} \min_{U(i)} \quad & w_2 \cdot u(i)^T B(i)^T B(i) u(i) \\ & + [w_1 K - 2w_2 B(i) V_{opt,i+1}^2] u(i) \\ \text{subject to} \quad & 0 \leq u(i) \leq u_{i,max} \\ & B(i) u(i) \leq v_{max} - A(i) X(i) + D(i) \end{aligned} \quad (19)$$

where $u_{i,max}$ is the upper boundary for u_i , v_{max} denotes the maximum speed allowed at time $i+1$ to ensure safety driving distance

$$v_{max} = (\Delta D(i+1)^* - l)/h \quad (20)$$

where $\Delta D(i+1)^*$ denotes the estimated spacing at time $i+1$ based on current spacing and current speed for both vehicles by assuming constant acceleration for the preceding vehicle:

$$\Delta D(i+1)^* = \Delta D + \left(\frac{v_{pre}(i) + v_{pre}(i+1)}{2} - v(i) \right) \cdot \Delta t \quad (21)$$

where $v_{pre}(i)$ denotes the speed of the preceding vehicle at time i .

Based on the above local speed adaption flow, we can define a vehicle status indicator vst at each adaption for tracking the vehicle status throughout the local adaption process

$$vst = \begin{cases} 1, & \text{if } d_i \geq d_{follow} \\ 2, & \text{if } d_i < d_{follow} \text{ and } d_{i,adj} \geq d_{follow} \\ 3, & \text{if } d_i < d_{follow} \text{ and } d_{i,adj} < d_{follow} \\ & \text{and } os_i = 1 \\ 4, & \text{if } d_i < d_{follow} \text{ and } d_{i,adj} < d_{follow} \text{ and} \\ & os_i = 0 \text{ and } os_{adj} = 1 \\ 5, & \text{if } d_i < d_{follow} \text{ and } d_{i,adj} < d_{follow} \text{ and} \\ & os_i = 0 \text{ and } os_{adj} = 0 \end{cases} \quad (22)$$

where os_i/os_{adj} is the indicator parameter to denote if the local optimization is solvable at the current/adjacent lane.

The local optimization described in (19) has the standard form of quadratic programming, which can be solved using commonly used methods such as interior point method. This form significantly reduces computational complexity of local optimization. As can be shown in [33], quadratic programming can be efficiently implemented using a high-throughput floating-point Field-Programmable Gate Array (FPGA) with operating frequency over 100MHz and a typical chip size of 30 cm^2 .

However, local optimization may fail to converge under some specific circumstances, e.g., a sudden change of lane from a vehicle on the adjacent lane without considering safety distance on the current lane. In such case, we need to force the vehicle to slow down to avoid collision. As shown in Fig. 5, when local optimization is unsolvable on the current and adjacent lanes, then we will force the vehicle to brake by imposing $V_{local}(i+1) = \max(0, V_{prec}(i+1) - V_m)$,

where V_m is a user-defined parameter to ensure the distance from preceding vehicle increases at the next time step: $0 \leq V_m \leq V_{prec}(i+1)$. The selection of V_m is a tradeoff between fuel consumption and safety. A smaller value of V_m will result in less fuel consumption in the emergent braking process while a larger value of V_m will result in larger distance at the expense of increasing fuel consumption. An example of brake situation is illustrated in Fig. 6(b).

IV. NUMERICAL EXAMPLE

The proposed ecological driving system for CAV using the proposed control hierarchy was illustrated based on simulation analysis in VISSIM. Recognizing the fact that a simulated network can truly reflect the reality only if it is well calibrated, we collected the field data at MD 100, Maryland and conducted a calibration for the VISSIM network. By observing the data at the study site of Maryland, the moderate traffic scenarios (10-20 vehicles/km/lane) in which the proposed model is more applicable usually happen after the peak-periods and can last about 1.5 hours. So the percentage of time for moderate traffic is around 12.5% (3 hours per day). For simulating the on-line operational procedure, we used the VISSIM-COM interface to develop a program to execute the local adaption function using VB.NET and the MYSQL database. During the simulation, the program detects and records the real-time traffic information and then adjusts the target vehicle's trajectory. The road condition and vehicle parameters used in our study are the following: $S = 5000m$, $\Delta S = 25m$, $n = 200$, $T_{max} = 220Nm$, $F_{max} = 3120N$, $f_r = 8$, $N_{fr} = 0.9$, $r_w = 0.25m$, $m = 3000kg$, $g = 9.8m/s^2$, $C_r = 0.01$, $\rho = 1.225$, $C_d = 0.3$, $A_d = 0.5m^2$, $\theta(t) = 0$. We set $w_1 = 10^8$ and $w_2 = 1$ which give the best balance between driving time and fuel consumption [30]. The speed limit of the considered distance is set to $90km/h = 25m/s$. We predicted our traffic state (speed and density) using the macroscopic model and the rolling-horizon control logic as described in Section III-A. The predicted traffic speed is then smoothed and used as target speed profile for long-term optimization. The blue curve in Fig. 7 shows the traffic speed $\hat{V}(s_i, t)$, $i = 1, \dots, 200$ predicted by our macroscopic model for the entire considered 200 segments. We then smoothed $\hat{V}(s, t)$ using a Gaussian-weighted moving average filter to produce a more realistic and trackable traffic speed profile \hat{V}_s , as shown by the orange curve in Fig. 7, which will be used as the new smoothed target speed profile in our global optimization.

A. Long-Term Optimization Using GA

Once traffic speed is predicted, we perform long-term optimization using GA as shown in (15) by setting $\hat{V}_{max}(s, t) = \hat{V}(s, t) + 1.39m/s$, and $\hat{V}_{min}(s, t) = \hat{V}(s, t) - 1.39m/s$ to ensure that the vehicle is at most $1.39m/s = 5km/h$ different from the current average traffic in order not to block the traffic. The two red curves in Fig. 7 represents the speed boundaries $\hat{V}_{min}(s, t)$ and $\hat{V}_{max}(s, t)$ using \hat{V}_s as target speed profile. The long-term optimization is then performed as described in Section III-B. The initial optimal speed $V_{opt}(0)$ is set to be equal to $\hat{V}_s(0)$. Once the optimization is performed and

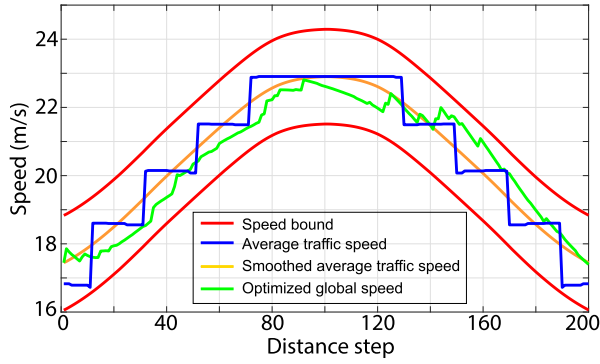


Fig. 7. Speed profile from global optimization as a function of distance steps.

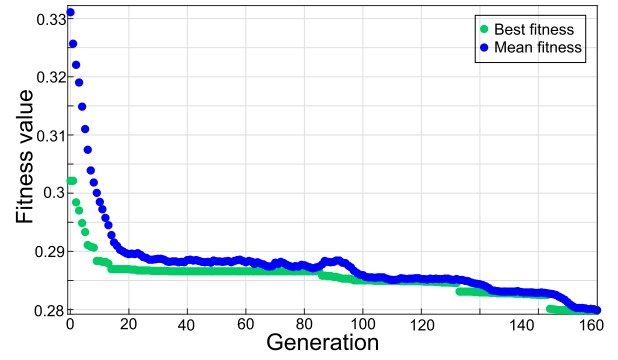


Fig. 9. Genetic algorithm performance in global optimization.

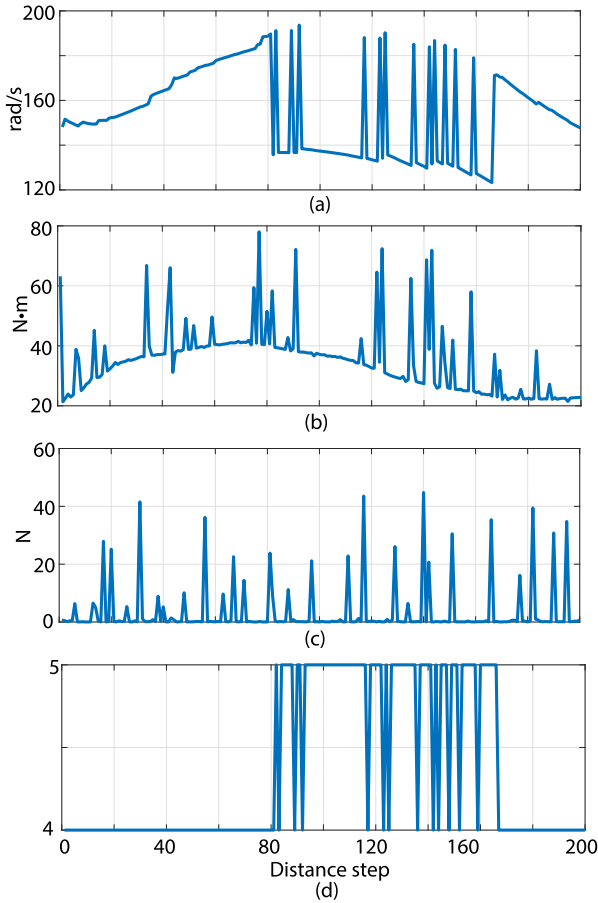


Fig. 8. Global optimization profile for (a) engine speed ω_e , (b) engine torque T_e , (c) brake force F_{brake} , and (d) gear number.

U_{opt} is computed, the global speed profile V_{opt} is computed as specified in (16).

The green curve in Fig. 7 shows the optimized global speed profile V_{opt} obtained by long-term optimization result U_{opt} . It can be observed that the optimal global speed profile is within our upper/lower boundaries shown by the red curves, and it generally follows the smoothed predicted traffic speed profile shown by the orange curve. Fig. 8 shows the vehicle powertrain parameters ω_e and T_e , brake force F_{brake} , and gear number profiles plotted as a function of distance steps

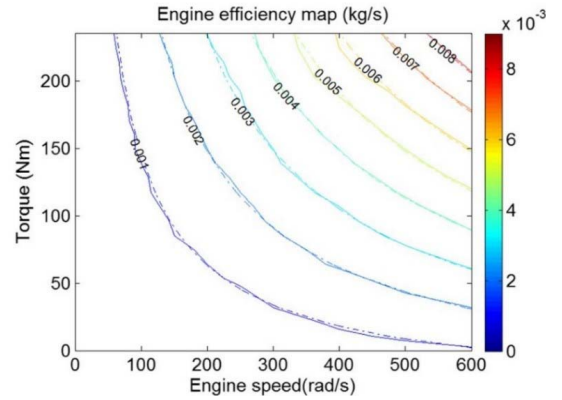


Fig. 10. Comparison of fuel maps using Willans line model (dashed curve) and Autonomie (solid curve) [30].

as a result of global optimization. Fig. 9 shows the GA performance plot with green dots representing the best fitness values in each GA generation and blue dots representing the mean fitness values. The GA achieved convergence after 160 generations, and the total computing time for GA in global optimization is 28s for an Intel Xeon CPU at 3.4GHz and a RAM of 32GB.

To provide a more accurate estimation of the fuel consumption using the proposed approach, we have used a fuel map generated from Autonomie to compute the fuel consumption. Fig. 10 shows a comparison of fuel maps computed using Willans line model (dashed curve) and Autonomie (solid curve) as shown in [30]. It can be observed that the Willans line model curve generally follows well the one obtained from Autonomie. The 2nd column of Table II shows the fuel consumption, traveling time, and average speed obtained from the proposed approach using Willans line model, and the 3rd column shows the results using Autonomie fuel map based on the optimized powertrain parameters from global optimization. It can be observed that the resulted fuel consumption are very close to each other with an error of 0.7%, which justifies the use of approximated Willans line model in our approach. For the rest of the paper, the fuel consumption results are calculated from Autonomie fuel map.

To compare the effectiveness of the proposed approach with state-of-the-art methods, we used the Gipps' car following

TABLE II
GLOBAL FUEL CONSUMPTION AND TRAVELING TIME COMPARISON

	Proposed with Willans line model	Proposed with fuel map from Autonomie	Average traffic	Approach in [15]
Fuel consumption (<i>kg</i>)	0.28	0.278	0.29	0.3
Traveling time (<i>s</i>)	246	246	242	244
Average speed (<i>m/s</i>)	20.3	20.3	20.6	20.5

model for all other vehicles during the trip in the VISSIM simulator, and we randomly selected 20 vehicles from the generated traffic in the simulator and recorded the speed profiles of these vehicles in the same 5000*m* traveling distance to compute the fuel consumption. For comparison purpose, we assume that all the 20 selected vehicles have the same powertrain model as the one under study.

The 4th column in Table II shows the average result from the 20 randomly selected vehicles as discussed before. It can be observed that our long-term optimization provides smaller fuel consumption as compared to the average value of the 20 selected vehicles. In order to show the statistical significance of this fuel saving, we performed a two-sample one-tailed *t*-test by considering the null hypothesis that the average fuel consumption of the 20 selected vehicles is equal to the value obtained using the proposed approach. The *t*-test result suggested that this null hypothesis is rejected at 5% significance level, which confirmed that the fuel consumption incurred from the proposed approach is smaller than other vehicles on the same trip with statistical significance.

We also made a comparison with the approach presented in [15], where powertrain parameters T_e and ω_e are selected such that the fuel consumption rate \dot{m}_{fuel} is minimized while the speed constraints are respected at each segment. The 5th column of Table II shows the result obtained using the approach in [15]. It can be observed that our long-term global optimization model provides the smallest fuel consumption with comparable average speed. The comparison results from Table II justify the need for optimizing target profile in the long-term global optimization.

B. Local Adaption Results

1) Local Adaption Using Optimized Global Speed Profile:

Once the optimized global speed profile V_{opt} is obtained from the long-term global optimization, we then perform local adaption as described in Section III-C. We set the local adaption time step $\Delta t = 1s$, i.e., local adaption is repeated every 1*s*, and the safety distance threshold $d_{follow} = 50m$.

In additional to the predicted traffic flow, at every time step, we insert a lane change probability for each of the considered vehicle. As demonstrated in [34], the probability of driver's discretionary lane change can be modeled by a binary logit model as a function of explanatory variables affecting decision and a random variable with normal distribution. Based on the empirical estimation from [34] and without loss of generality, we insert a discretionary lane change probability of 0.01.

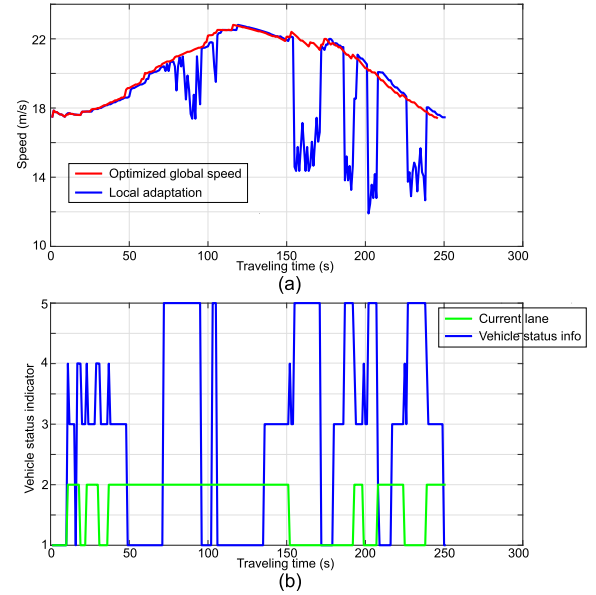


Fig. 11. Local adaption results: (a) local adapted speed profile and (b) vehicle status and lane information.

TABLE III
FUEL CONSUMPTION COMPARISON FOR LOCAL ADAPTION

	Proposed	Average traffic	Approach in [15]	Trajectory based on smoothed traffic profile
Fuel consumption (<i>kg</i>)	0.34	0.36	0.36	0.35
Traveling time (<i>s</i>)	252	254	254	253
Average speed (<i>m/s</i>)	19.8	19.7	19.7	19.8

Since local adaption is performed in time scale, the results are shown in time-scale in Fig. 11. The blue curve in Fig. 11(a) shows the local adapted speed profile and the red curve shows the target optimized global speed profile V_{opt} in time scale. It can be observed that local speed profile has several abrupt speed reductions. To gain some insight about these reductions, the blue curve in Fig. 11(b) shows the vehicle status indicator value vst as defined by (22) and the green curve shows the lane number on which the vehicle travels at each time point. By combining Fig. 11(a) and (b), it can be observed that abrupt speed reductions mainly occur when the vehicle status information is 5, i.e., the distance from the preceding vehicle is less than d_{follow} and local optimization is unsolvable for both lanes. Thus, the vehicle has to brake to avoid collision as described in Section III-C. When the distance from the preceding vehicle becomes greater than d_{follow} or local optimization becomes solvable, our local adaption can quickly adapt the local speed to global optimal speed profile, which ensures minimum fuel consumption while keeping the safety driving distance.

The 2nd column of Table III shows the updated fuel consumption and traveling time information using local adapted speed profile shown by the blue curve in Fig. 11(a).

TABLE IV
FUEL CONSUMPTION VALUES AND DRIVING TIMES
FOR DIFFERENT w_2 VALUES WITH $w_1 = 10^8$

	$w_2 = 0.5$	$w_2 = 1$	$w_2 = 5$
Fuel consumption (kg)	0.34	0.34	0.36
Traveling time (s)	251	251	250

By comparing the 2nd column of Table III to the 2nd column of Table II, it can be observed that the fuel consumption from local speed profile is slightly higher than that obtained from optimized global speed profile, due to the abrupt speed reductions discussed before. The 3rd column in Table III shows the average local adaption results from the 20 randomly selected vehicles as discussed before. It can be observed that our approach still provides smaller fuel consumption as compared to the average value of the 20 selected vehicles in the local adaption.

As shown in (19), the choice of w_1 and w_2 is a tradeoff between the fuel consumption and how close the resulting speed profile is to the optimized global speed. Table IV shows different fuel consumption values and driving times for different w_2 values with w_1 fixed at 10^8 . It can be observed that since the number of times when local adaption is needed during the trip is relatively small, the impact of w_1 and w_2 on the final fuel consumption and driving time is limited.

C. Comparison With Global Target Profile Based on Smoothed Average Traffic

In order to illustrate the advantages of using predicted traffic flow as global speed profile, we have performed local adaption using the smoothed average traffic profile as shown by the orange curve in Fig. 7 as the global target profile. The 5th column of Table III shows the results based on smoothed average traffic profile. It can be observed that the fuel consumption using smoothed average traffic profile has a slightly higher fuel consumption as compared to the proposed approach with comparable traveling speed. Fig. 12 shows the local adaption results based on smoothed average traffic profile. The red curve in Fig. 12(a) is the time-domain equivalent speed profile of the orange curve in Fig. 7, and the blue curve in Fig. 12(a) shows the adapted local speed profile. The vehicle status indicator and lane information are shown in Fig. 12(b).

D. Comparison With Single-Lane Optimization

One of the major contributions of the proposed approach is the consideration of lane change during optimization. To illustrate the significance of considering lane change, we have performed optimization in a single lane without lane change function. Fig. 13 shows local adaption results without lane change function. As can be observed, more abrupt speed reductions are observed as compared to Fig. 11. The fuel consumption after local adaption based on single-lane optimization is $0.38kg$. This result shows that single-lane optimization consumes more fuel, corroborating the necessity of developing lane change function in the optimization.

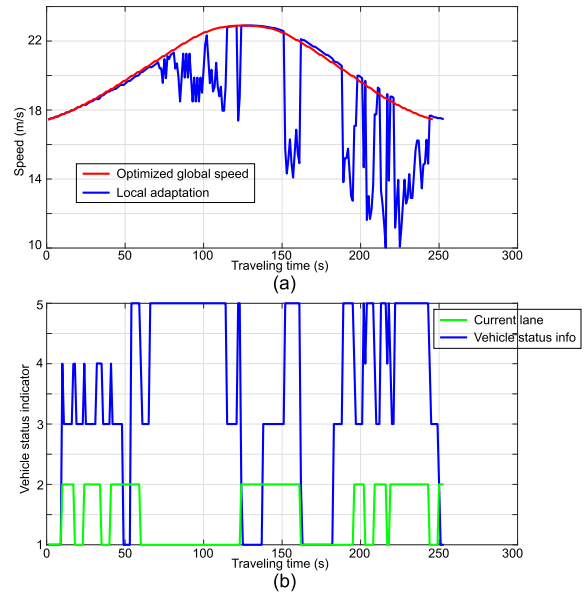


Fig. 12. Local adaptation results using smoothed average traffic: (a) local adapted speed profile and (b) vehicle status and lane information.

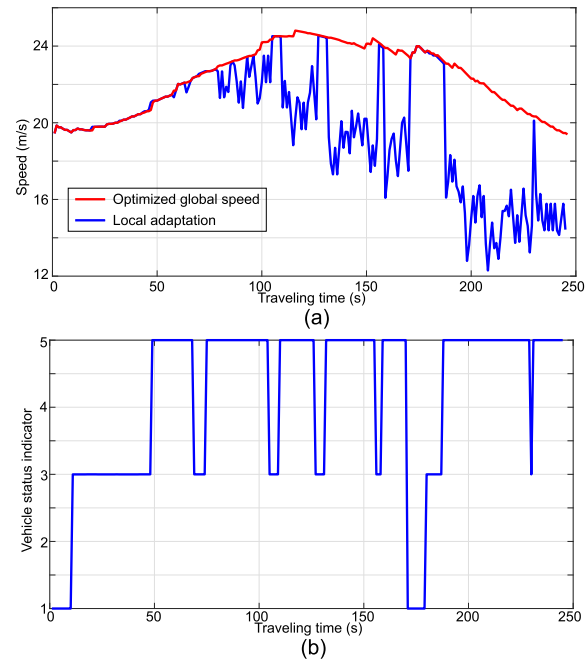


Fig. 13. Local adaptation results without lane change function: (a) local adapted speed profile and (b) vehicle status indicator information.

E. Road Grade Sensitivity Analysis

The final fuel consumption for the given traveling distance is impacted by several environmental and vehicular factors, including road grade, rolling resistance coefficient, vehicle mass, etc. The road grade parameter θ was set to 0 previously. To show how fuel consumption is impacted by θ , we have performed a road grade sensitivity analysis. As demonstrated in [35], the road grade can be accurately modeled by a piecewise linear model. Thus, for the purpose of this study and without loss of generality, we employed a piecewise linear model composed of two linear functions with opposite slope

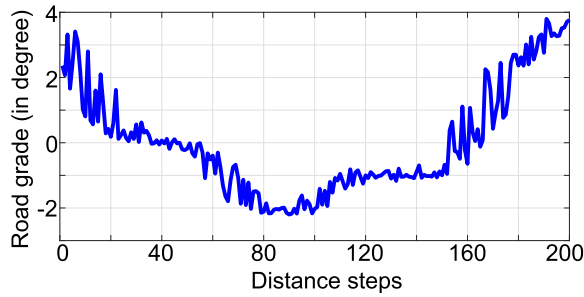


Fig. 14. Road grade generated by piecewise linear model with 0 mean.

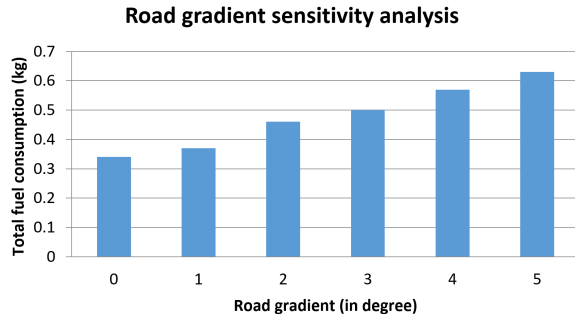


Fig. 15. Road grade sensitivity analysis.

signs and random Gaussian noise as illustrated in Fig. 14, to represent road grade variation throughout the trip. The grade curve shown in Fig. 14 is plotted in degree as a function of distance steps. The mean value of the grade curve in Fig. 14 is set to 0. We then adjusted the mean value (in degree) of the generated grade curve by adding a constant to the curve to observe how fuel consumption varies as a function of mean grade value.

Fig. 15 shows the fuel consumption for different grade mean values ranging from 0° to 5° . It can be observed that more fuels are consumed as the road becomes steeper, and the fuel consumption difference can be 0.29kg between 0° and 5° mean grade values. This observation justifies the consideration of road grade information in the fuel consumption computation model.

V. CONCLUSIONS

In this work, we proposed a two-stage hierarchical framework for minimizing fuel consumption in a CAV environment. Our proposed framework included traffic state prediction, global target speed optimization and local speed adaption. The predicted traffic state served as the target speed in the optimization process and the optimization function was activated once new traffic state predictions were available. The second stage, local speed adaption was designed to dynamically adjust vehicle speed and make lane-changing decision based on local driving conditions. The experimental results confirmed the effectiveness of the proposed system in reducing fuel consumption. Further comparisons with different models also highlighted the need of considering traffic state information in the first-stage optimization and lane-changing decision module in the local adaption function.

REFERENCES

- [1] World Energy Council. *World Energy Scenarios 2007: Transport Technologies and Policy Scenarios*. Accessed: Mar. 6, 2017. [Online]. Available: <https://www.worldenergy.org/publications/2007/transport-technologies-and-policy-scenarios/>
- [2] *Annual Energy Outlook 2010 With Projections to 2035*, document DOE/EIA-0383(2010), Energy Information Administration, Washington, DC, USA, 2010.
- [3] Y. Fujiki, H. Takemoto, and K. Enomoto, "Apparatus for coaching a driver for driving operation to improve fuel efficiency," U.S. Patent 2011 0 210 838 A1, Sep. 17, 2009.
- [4] S. Park, H. Rakha, K. Ahn, and K. Moran, "Predictive eco-cruise control: Algorithm and potential benefits," in *Proc. IEEE Forum Integr. Sustain. Transp. Syst.*, Vienna, Austria, Jun./Jul. 2011, pp. 394–399.
- [5] K. Boriboonsomsin and M. Barth, "Impacts of road grade on fuel consumption and carbon dioxide emissions evidenced by use of advanced navigation systems," *Transp. Res. Rec., J. Transp. Res. Board*, vol. 2139, pp. 21–30, 2009.
- [6] K. Boriboonsomsin, A. Vu, and M. Barth, "Eco-driving: Pilot evaluation of driving behavior changes among U.S. drivers," Univ. California Transp. Center, Riverside, CA, USA, Tech. Rep. UCTC-FR-2010-20, 2010.
- [7] I. Berry, "The effects of driving style and vehicle performance on the real-world fuel consumption of us light-duty vehicles," Ph.D. dissertation, Massachusetts Inst. Technol., Cambridge, MA, USA, 2010.
- [8] Y. Takada, S. Ueki, A. Saito, N. Sawazu, and Y. Nagatomi, "Improvement of fuel economy by eco-driving with devices for freight vehicles in real traffic conditions," SAE Tech. Paper 2007-01-1323, 2007.
- [9] Q. Jin, G. Wu, K. Boriboonsomsin, and M. J. Barth, "Power-based optimal longitudinal control for a connected eco-driving system," *IEEE Trans. Intell. Transp. Syst.*, vol. 17, no. 10, pp. 2900–2910, Oct. 2016.
- [10] J. N. Hooker, "Optimal driving for single-vehicle fuel economy," *Transp. Res. A, Gen.*, vol. 22, no. 3, pp. 183–201, 1988.
- [11] M. A. S. Kamal, M. Mukai, J. Murata, and T. Kawabe, "Ecological vehicle control on roads with up-down slopes," *IEEE Trans. Intell. Transp. Syst.*, vol. 12, no. 3, pp. 783–794, Sep. 2011.
- [12] N. J. Kohut, J. K. Hedrick, and F. Borrelli, "Integrating traffic data and mode predictive control to improve fuel economy," in *Proc. 12th IFAC Symp. Control Transp. Syst.*, Redondo Beach, CA, USA, 2009, pp. 155–160.
- [13] G. De Nunzio, C. C. de Wit, P. Moulin, and D. Di Domenico, "Eco-driving in urban traffic networks using traffic signal information," in *Proc. IEEE Conf. Decision Control*, Florence, Italy, Dec. 2013, pp. 892–898.
- [14] E. Hellström, J. K. Åslund, and L. Nielsen, "Design of an efficient algorithm for fuel-optimal look-ahead control," *Control Eng. Pract.*, vol. 18, no. 11, pp. 1318–1327, 2010.
- [15] J. Hu, Y. Shao, Z. Sun, M. Wang, J. Bared, and P. Huang, "Integrated optimal eco-driving on rolling terrain for hybrid electric vehicle with vehicle-infrastructure communication," *Transp. Res. C, Emerg. Technol.*, vol. 68, pp. 228–244, Jul. 2016.
- [16] B. Dafflon, J. Vilca, F. Gechter, and L. Aduane, "Adaptive autonomous navigation using reactive multi-agent system for control law merging," *Procedia Comput. Sci.*, vol. 51, pp. 423–432, 2015.
- [17] R. Scarinci and B. Heydecker, "Control concepts for facilitating motorway on-ramp merging using intelligent vehicles," *Transp. Rev.*, vol. 34, no. 6, pp. 775–797, 2014.
- [18] M. Wang, W. Daamen, S. P. Hoogendoorn, and B. van Arem, "Rolling horizon control framework for driver assistance systems. Part I: Mathematical formulation and non-cooperative systems," *Transp. Res. C, Emerg. Technol.*, vol. 40, pp. 271–289, Mar. 2014.
- [19] M. Wang, W. Daamen, S. P. Hoogendoorn, and B. van Arem, "Rolling horizon control framework for driver assistance systems. Part II: Cooperative sensing and cooperative control," *Transp. Res. C*, vol. 40, pp. 290–311, Mar. 2014.
- [20] Z. Huang, Q. Wu, J. Ma, and W. Tian, "Modeling and simulation of cooperative strategies for vehicle platoon longitudinal control," in *Proc. CICTP Safe, Smart, Sustain. Multimodal Transp. Syst.*, 2014, pp. 498–512.
- [21] P. Nyitchogna, L. Nouveliere, O. Orfila, S. Glaser, and S. Mammari, "Impact of full speed range ACC on the traffic, the safety and the energy consumption," in *Proc. 5th Conf., Transp. Solutions Res. Deployment Transp. Res. Arena (TRA)*, 2014, pp. 1–10.
- [22] P. Ioannou, "Evaluation of the effects of intelligent cruise control vehicles in mixed traffic," California Partners Adv. Transit Highways, Richmond, CA, USA, Tech. Rep. UCB-ITS-PRR-2003-2, 2003.

- [23] A. Girault, "A hybrid controller for autonomous vehicles driving on automated highways," *Transp. Res. C, Emerg. Technol.*, vol. 12, no. 6, pp. 421–452, 2004.
- [24] M. A. M. Zulkefli, J. Zheng, Z. Sun, and H. X. Liu, "Hybrid powertrain optimization with trajectory prediction based on inter-vehicle-communication and vehicle-infrastructure-integration," *Transp. Res. C, Emerg. Technol.*, vol. 45, pp. 41–63, Aug. 2014.
- [25] Y. Wang, H. Zhang, and Z. Sun, "Optimal control of the transient emissions and the fuel efficiency of a diesel hybrid electric vehicle," *Proc. Inst. Mech. Eng., D, J. Automobile Eng.*, vol. 227, no. 11, pp. 1546–1561, 2013.
- [26] F. Mensing, R. Trigui, and E. Bideaux, "Vehicle trajectory optimization for application in ECO-driving," in *Proc. IEEE Vehicle Power Propuls. Conf. (VPPC)*, Chicago, IL, USA, Sep. 2011, pp. 1–6.
- [27] H. T. Luu, L. Nouvelière, and S. Mammari, "Ecological and safe driving assistance system: Design and strategy," in *Proc. IEEE Intell. Vehicle Symp. (IV)*, San Diego, CA, USA, Jun. 2010, pp. 129–134.
- [28] J. Jing, "Vehicle fuel consumption optimization using model predictive control based on v2v communication," M.S. thesis, Dept. Elect. Comput. Sci., Ohio State Univ., Columbus, OH, USA, 2014.
- [29] S. Xu, K. Deng, S. E. Li, S. Li, and B. Cheng, "Legendre pseudospectral computation of optimal speed profiles for vehicle eco-driving system," in *Proc. IEEE Intell. Vehicles Symp.*, Dearborn, MI, USA, Jun. 2014, pp. 1103–1108.
- [30] H. Lim, W. Su, and C. Mi, "Distance-based ecological driving scheme using a two-stage hierarchy for long-term optimization and short-term adaptation," *IEEE Trans. Veh. Technol.*, vol. 66, no. 3, pp. 1940–1949, Mar. 2016.
- [31] A. Messmer and M. Papageorgiou, "METANET: A macroscopic simulation program for motorway networks," *Traffic Eng. Control*, vol. 31, no. 8, pp. 466–470, 1990.
- [32] G. Rizzoni, L. Guzzella, and B. M. Baumann, "Unified modeling of hybrid electric vehicle drivetrains," *IEEE/ASME Trans. Mechatronics*, vol. 4, no. 3, pp. 246–257, Sep. 1999.
- [33] J. Jerez, G. A. Constantinides, and E. C. Kerrigan, "An FPGA implementation of a sparse quadratic programming solver for constrained predictive control," in *Proc. 19th ACM/SIGDA Int. Symp. Field Program. Gate Arrays*, 2011, pp. 209–218.
- [34] K. Ahmed, "Modeling drivers' acceleration and lane changing behavior," Ph.D. dissertation, Dept. Civil Environ. Eng., Massachusetts Inst. Technol., Cambridge, MA, USA, 1999.
- [35] P. Sahlholm and K. Johansson, "Segmented road grade estimation for fuel efficient heavy duty vehicles," in *Proc. IEEE Conf. Decision Control*, Dec. 2010, pp. 1045–1050.

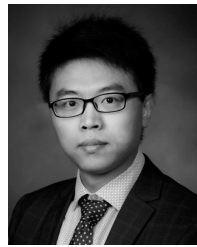


Ke Huang (S'10–M'12) received the B.S. and M.S. degrees in electrical engineering from Joseph Fourier University in 2006 and 2008, respectively, and the Ph.D. degree in electrical engineering from University of Grenoble, Grenoble, France, in 2011.

He was a Post-Doctoral Research Associate with University of Texas at Dallas, Richardson, TX, USA, from 2012 to 2014. In 2014, he joined the Department of Electrical and Computer Engineering with San Diego State University, San Diego, CA, USA, where he is currently an Assistant Professor. His

research interests include intelligent vehicles, very-large-scale integration testing and security, and computer-aided design of integrated circuits.

Dr. Huang was a recipient of the Best Paper Award from the 2015 IEEE VLSI Test Symposium (VTS'15) and the Best Paper Award from the 2013 Design Automation and Test in Europe (DATE'13) Conference.



Xianfeng Yang received the B.S. degree in civil engineering from Tsinghua University, Beijing, China, in 2009, and the M.S. and Ph.D. degrees in civil engineering from University of Maryland at College Park, College Park, MD, USA, in 2012 and 2015, respectively.

He was an Assistant Professor of transportation engineering with San Diego State University for two years. He is an Assistant Professor with the Department of Civil and Environmental Engineering, The University of Utah. He is the Co-Director of the Utah Traffic Lab, which is sponsored by multiple funding agencies, such as the Utah Department of Transportation, the National Science Foundation, the U.S. Department of Transportation, the Federal Highway Administration, the Utah Transit Authority, and two University Transportation Centers including the National Institute for Transportation and Communities and Mountain-Plains Consortium. He has published over 50 journals and conference papers. His current research interests include developing dynamic evacuation systems, designing traffic incident management systems, and using connected vehicle technology in traffic operations. He has been a member of the Traffic Signal System Committee of the Transportation Research Board.



Yang (Carl) Lu received the B.S. degree in control from Beijing Jiaotong University, and the M.S. and Ph.D. degrees in transportation from University of Maryland at College Park, College Park, MD, USA. He is currently an Urban Transport Consultant with Transport and ICT, World Bank, USA. His research interests include active traffic management, big data applications in transportation, intelligent transportation system, and traffic operations and management in general.

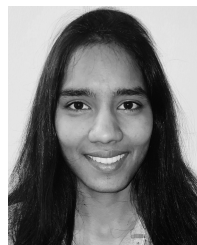


Chungting Chris Mi (S'00–A'01–M'01–SM'03–F'12) received the B.S.E.E. and M.S.E.E. degrees in electrical engineering from Northwestern Polytechnical University, Xi'an, China, and the Ph.D. degree in electrical engineering from University of Toronto, Toronto, ON, Canada.

He was with General Electric Company, Peterborough, ON, Canada, and a Professor with the Department of Electrical and Computer Engineering, University of Michigan, Dearborn, MI, USA. He is a Professor of electrical and computer

engineering and the Director of the Department of Energy-funded Graduate Automotive Technology Education Center for Electric Drive Transportation, San Diego State University, San Diego, CA, USA.

His research interests include electric drives, power electronics, electric machines, renewable-energy systems, and electrical and hybrid vehicles. He has conducted extensive research and has published over 100 journal papers. He is an Area Editor of IEEE TRANSACTIONS ON VEHICULAR TECHNOLOGY and an Associate Editor of IEEE TRANSACTIONS ON POWER ELECTRONICS and IEEE TRANSACTIONS ON INDUSTRY APPLICATIONS.



Prathyusha Kondlapudi is currently pursuing the master's degree with the Department of Electrical and Computer Engineering, San Diego State University, USA. Her research interests include very-large-scale integration hardware implementation of eco-driving control algorithms.